Theoretical study of the electronic properties of PrM_2B_2C (M=Co,Ni,Pt)

Donald H. Galvan,[1] A. Durán,[1] A. Posada Amarillas,[2] and R. Escudero[3]
[1]*Centro de Ciencias de la Materia Condensada, Universidad Nacional Autónoma México, Apartado Postal 2681, CP 22800, Ensenada, B. C., México*
[2]*Departamento de Investigaciones en Física, Universidad de Sonora, Apartado Postal 5-088, CP 83190 Hermosillo, Sonora, México*
[3]*Instituto de Investigaciones en Materiales, Universidad Nacional Autónoma de México, Apartado Postal 70-360, México, D. F., CP 04510, México*
(Received 21 September 2006; published 26 December 2006)

Full substitution of Ni by the transition metals Co and Pt in PrM_2B_2C (M=Ni,Co,Pt) is analyzed using tight binding within the extended Huckel method. Electronic structure calculation, total and projected density of states (PDOS), Mulliken population, and crystal orbital overlap population analysis were examined in order to elucidate the absent or presence of superconductivity. Band-structure calculation shows small differences in Pr/Ni and Pr/Co compounds. The total and PDOS crossing the Fermi energy (E_F) is located in a valley and is dominated by $-d$ states, which are principally responsible for the metallic character in both compounds. For Pr/Pt compound, the band structure as well as the total and PDOS are fully different, since two sets of bands, the $-f$ and $-d$ bands, are highly localized at the E_F, contributing both bands to the electronic conduction. Besides, weak hybridization with important contribution of the C $-p$ state is observed in Pr/Pt with respect to the Pr/Ni and Pr/Co compound, where in these last compounds, the C $-p$ contribution is null. Furthermore, Mulliken population analysis and average net charge indicated unfilled $-d$ orbital with charge transference inside the M_2B_2 layer for Pr/Ni(Co). The situation is totally different for Pr/Pt superconductor compounds, since an almost filled $-d$ orbital and homogeneous charge distribution were observed. These theoretical evidences suggest that the absence of the superconductivity in Pr/Ni and Pr/Co are connected by the remarkable instabilities between $-d$, $-p$, and $-f$ states, with respect to that observed in the superconductor $PrPt_2B_2C$ compounds.

DOI: 10.1103/PhysRevB.74.245121 PACS number(s): 71.15.Ap, 71.20.Eh, 71.20.−b

I. INTRODUCTION

Intermetallic borocarbides with formula RM_2B_2C (R=Y, lanthanides, M=Ni,Co,Pt,Pd,Rh) have been subject to extensive theoretical and experimental investigation, due fundamentally to the fact that in certain combination of R and M elements, the magnetic and superconducting ordering coexist on a microscopic scale.[1–4] At present, it is particularly interesting to understand the mechanism related to absence or coexistence of these antagonistic phenomena.

Electronic band-structure calculations suggest that these materials are conventional superconductors with relatively high density of state at the Fermi level.[5,6] The disappearance of the superconductivity on moving from small to large lanthanides in RNi_2B_2C series has been attributed theoretically to a decrease in the density of state (DOS) and to the electron-phonon coupling at the Fermi level caused by structural factors, mainly by the overlap of the Ni-Ni environment. Within this framework, the DOS at the Fermi level shows a peak in the lanthanide series, perhaps related to superconductivity according to the BCS; on the contrary, the nonsuperconducting members present a valley in the DOS at the Fermi level.[7–9] Also, we have found that the superconducting transition (Tc) varies with the rare earth, suggesting that the magnetic rare earth sublattice has influence on the superconducting properties.[4,10] On the other hand, it was found that the complete substitution of Ni by Pt in $LaPt_2B_2C$ and $PrPt_2B_2C$ compounds are superconducting at 10 and 6 K, respectively.[11] These compounds have attracted attention since they are the first superconducting systems with light rare earth elements in the $LuNi_2B_2C$-type structure. Thus, the role played by rare earth and transition metal sites in RM_2B_2C compounds is a dominant aspect in transport and superconducting properties.

For PrM_2B_2C (M=Ni, Co, and Pt) intermetallic compounds, it was found experimentally that the full substitution of Co by Ni yields minimal structural changes with similar transport properties, i.e., both are not superconductors and display magnetic ordering at low temperature.[12,13] On the other hand, the replacement of M by Pt induces significant changes in the internal crystal structure, with superconductivity present at about 6 K without magnetic ordering down to 1.8 K. In addition, specific heat measurement shows a slight enhancement in the Sommerfeld constant (γ) with respect to that of $LuNi_2B_2C$ compound.[14]

In this work, we have employed previous structural data extracted from single crystals in order to study the electronic structure of PrM_2B_2C (T=Ni, Co, and Pt) using Huckel tight-binding calculations. We also analyze the electronic structure by means of energy bands, total and projected density of states (PDOS), Mulliken population analysis, and crystal orbital overlap population (COOP), which will yield information regarding the electronic properties of the materials in question.

II. CRYSTAL STRUCTURE AND COMPUTATIONAL DETAILS

Here, we discuss concisely the main change in the lattice parameters, as well as the theoretical and computational de-

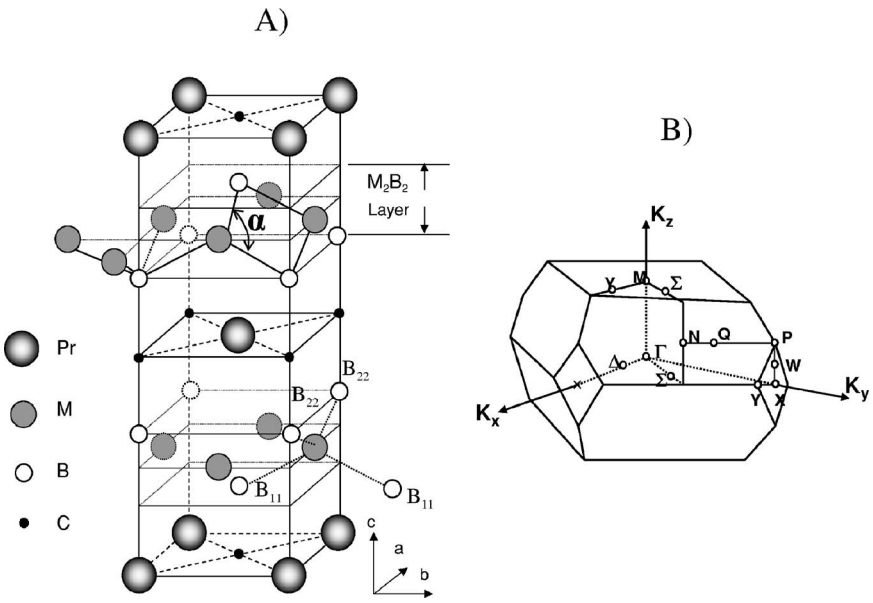

FIG. 1. (a) Crystal structure for PrM_2B_2C, with M=Ni, Co, and Pt. Internal angle α and M_2B_2 layer thickness normal to the c axis. (b) Wigner-Seitz cell for a bct configuration with the main point of the FBZ.

tails, employing a semiempirical methodology in order to calculate the band electronic structure for the three compounds under investigation.

Lattice parameters, metal-metal bond length, and the motion of the internal bonding parameters were taken from x-ray diffraction measurements on single crystals grown by our group.[15] The space group $I4/mmm$ (139) of the compounds PrM_2B_2C, M=Co,Ni,Pt (Pr/Co, Pr/Ni and Pr/Pt) were confirmed by the symmetric equivalent intensities measurements from rotation photographs. The Pr ion occupies the position 2(a) (0 0 0), M(=Co,Ni,Pt) 4(d) (1/2 0 1/4), C 2(b) (−1/2−1/2 0), and B 4(e) (0 0 z) with z=0.351(3), 0.350(5), and 0.362(9) for Ni, Co, and Pt, respectively. The unit cell is shown in Fig. 1(a) and contains 2 M, 2 B, 1 C, and 1 Pr atom. The structural parameters are listed and compared in Table I. It seems that the substitution of Ni by Co decreases slightly the unit cell volume in line as the basal plane parameter does. Note that the Co-Co distance is the shortest observed in the compounds under study. Nevertheless, the Ni-Ni and Co-Co distance are still larger than the corresponding M-M distances observed for the Co and Ni fcc metals (2.50 and 2.51 Å). On the other hand, the full substitution of Ni by Pt significantly modifies the c and a parameters, as expected from the large Pt ionic radii. In the internal MB_4 framework it is observed that the layer thickness (M_2B_2) increases about 2.7% and 19.4% when Ni is substituted by Co, and Ni by Pt, respectively. This behavior suggests significant weakness of the Pt-5d with neighbor B -2p covalent bonds, in addition to an increase of 7.7% in the c parameter for $PrPt_2B_2C$. This effect is reflected by the large B_{11}-M-B_{22} bond angle [α in Fig. 1(a)] changing from 103.33(7) for Pr/Ni to 104.43(12) for Pr/Co to 106.6(3)° for Pr/Pt, and also by the Pt_2B_2 layer thickness. In $PrPt_2B_2C$, the Pt-Pt distance of 2.7134(1) Å in the a-b plane is shorter than the atomic distance expected from the metallic Pt, 2.77 Å. This suggests a strong metal-metal bonding and an increase in the DOS with subsequent increase in the electron-phonon coupling, as was observed in the Ni-based superconductor intermetallic compounds.[5–7]

The band-structure calculations were carried out by means of the tight-binding method[16] within the extended Huckel[17] framework using the YAEHMOP[18] computer package with f orbitals. More details about the method are given elsewhere[19] and are omitted here for brevity.

The band structures for PrM_2B_2C (M=Co,Ni,Pt) were calculated using 105 k points, sampling the first Brillouin zone (FBZ). Figure 1(b) depicts the Wigner-Seitz cell for a body-centered-tetragonal (bct) configuration spanning from Γ (0 0 0) to X (0 $\pi/2a$ 0) to Y ($\pi/3a$ $\pi/2a$ 0) to M ($\pi/2a$ $\pi/2a$ 0) to Γ (0 0 0), which generates the FBZ. The atomic parameters employed in our calculations were obtained from Alvarez[20] and are summarized in Table II.

TABLE I. Structural parameters, selected interatomic distances (Å), and angles (°) for PrM_2B_2C at room temperature.

Compound	a (Å)	c (Å)	V (Å)	M-M (Å)	M_2B_2 Layer thickness (Å)	B_{11}-M-B_{22} (α angle) Tetrahedral angle (°)
$PrNi_2B_2C$	3.6996(2)	9.9885(8)	136.71(1)	2.6160(1)	2.026	103.33(7)
$PrCo_2B_2C$	3.6156(1)	10.3507(6)	135.31(1)	2.5566(1)	2.082	104.4(1)
$PrPt_2B_2C$	3.8373(1)	10.7610(9)	158.45(1)	2.7134(1)	2.424	106.6(3)

TABLE II. Atomic parameters used in the extended Huckel tight-binding calculations, H_{ii} (eV) and ς (valence orbital ionization potential and exponent of Slater-type orbitals). The $-d$ orbitals for Co (Ni/Pt) and Pr are given as a linear combination of two Slater-type orbitals. Each exponent is followed by a weighting coefficient in parentheses. A modified Wolfsberg-Helmholtz formula was used to calculate H_{ij}.[31]

Atom	Orbital	H_{ii}	ς_{i1}	C_1	ς_{i2}	C_2
Co	4*s*	−7.800	2.000			
	4*p*	−3.800	2.000			
	3*d*	−9.700	5.555	0.5550	1.9000	0.6678
Ni	4*s*	−7.800	2.100			
	4*p*	−3.700	2.100			
	3*d*	−9.900	5.750	0.5683	2.000	0.69920
Pt	6*s*	−9.070	2.554			
	6*p*	−5.475	2.554			
	5*d*	−12.590	6.013	06334	2.696	0.5513
Pr	6*s*	−7.420	1.400			
	6*p*	−4.650	1.400			
	5*d*	−8.080	2.735	0.7187	1.267	0.4449
	4*f*	−11.280	6.907	0.7354	2.639	0.4597
C	2*c*	−21.400	1.625			
	2*p*	−11.400	1.625			
B	2*s*	−15.200	1.300			
	2*p*	−8.500	1.300			

III. RESULTS AND DISCUSSION

A. Electronic properties

The most important features in the dispersion diagram for $PrNi_2B_2C$, $PrCo_2B_2C$, and $PrPt_2B_2C$ are depicted in Figs. 2(a)–2(c). The energy between −8 and −13 eV was selected because the Fermi level is highly localized in this range. It is interesting, from the electronic point of view, to highlight the bands that participate in the transport properties at the Fermi level. Throughout the manuscript we discuss Pr/Ni and Pr/Co together because experimentally, they show similar transport behavior and are not superconductors. The electronic structure shows small differences, as seen in Figs. 2(a) and 2(b). Here, the bands located in the energy range between ~10.7 eV and the Fermi level are mainly Ni(Co) $-d$ bands, which are hybridized with the B $-p$ states with a small admixture of C $-p$ states. These bands are mainly responsible of the metallic character in both systems. It is important to note that these bands are similarly located below E_f (at the Γ point) and cross it, presenting inflexion points at *X* and *M* direction of the FBZ. More information regarding the bands that cross the E_f are related to the Ni/Co atoms, which are in a tetrahedral coordination in the M_2B_2 layer. As a consequence, the crystal field breaks the degeneracy of the $-d$ orbital, providing two distinct sets of energy values in the crystal. One of them is of e_g symmetry and doubly degenerate (d_{x2-y2} and d_{z2}), while the other one is of t_{2g} symmetry and triply degenerate (d_{xy}, d_{xz}, and d_{yz}), e_g being lower in energy than the t_{2g} band. Notice that these bands [indicated by the arrows in Figs. 2(a) and 2(b)] had been identified by Felser[8] as being of antibonding ddσ^* character in RM_2B_2C (*R*=Lu, Th, and La; *M*=Ni and Pd) compounds. This antibonding ddσ^* has been split with a "width" major in Pr/Co in Pr/Ni compound; besides, this band gave rise to a shift of ~0.35 eV toward the conduction band, as seen between the *X* and *M* directions of the FBZ in Fig. 2(b). Furthermore, it is observed that one triply degenerated band (~10.75 eV) crosses the Fermi level and overlaps with the doubly degenerated bands (ddσ^*) at the *Y* direction of the FBZ. This effect is likely a consequence of the closer Co-Co distance compared with Ni-Ni distance (see Table I). In order to check the contribution to the total DOS of each band separately, we calculated the relative weights of the corresponding orbital. The results were as follows: for $PrCo_2B_2C$, the contribution from d_{x2-y2} was ≅6%, while d_{z2} was ≅7%, with a total contribution of the order of ≅13% to the total DOS. Meanwhile, for $PrNi_2B_2C$ the contribution from d_{x2-y2} was ≅8% and d_{z2} was ≅14%, with a total contribution of the order of ≅22%. Furthermore, the interaction of those bands at the Fermi level display symmetrical band dispersion in the Γ-*X* and *M*-Γ direction, suggesting three-dimensional metallic scattering with all atoms (mainly $-d$ and $-p$ electrons) participating at the Fermi level. Fisher *et al.*[21] have confirmed the quasi-isotropic metallic character in some Ni-based compounds, without discard, here similar to quasi-isotropic transport behavior in Pr/Ni and Pr/Co compounds. Thus, a decrease in the *a*-*b* plane with simultaneous increase of the *c* parameters yields a difference in the total DOS contribution, with a small difference in the separation between bands when Co substitutes the Ni ion. The structural distortion of the tetrahedral MB_4 framework produces a Peierls-type distortion commonly found in solid systems.[22] This type of structural distortion likely opens minigaps at some specific point of the FBZ, as is observed in some bands of the two

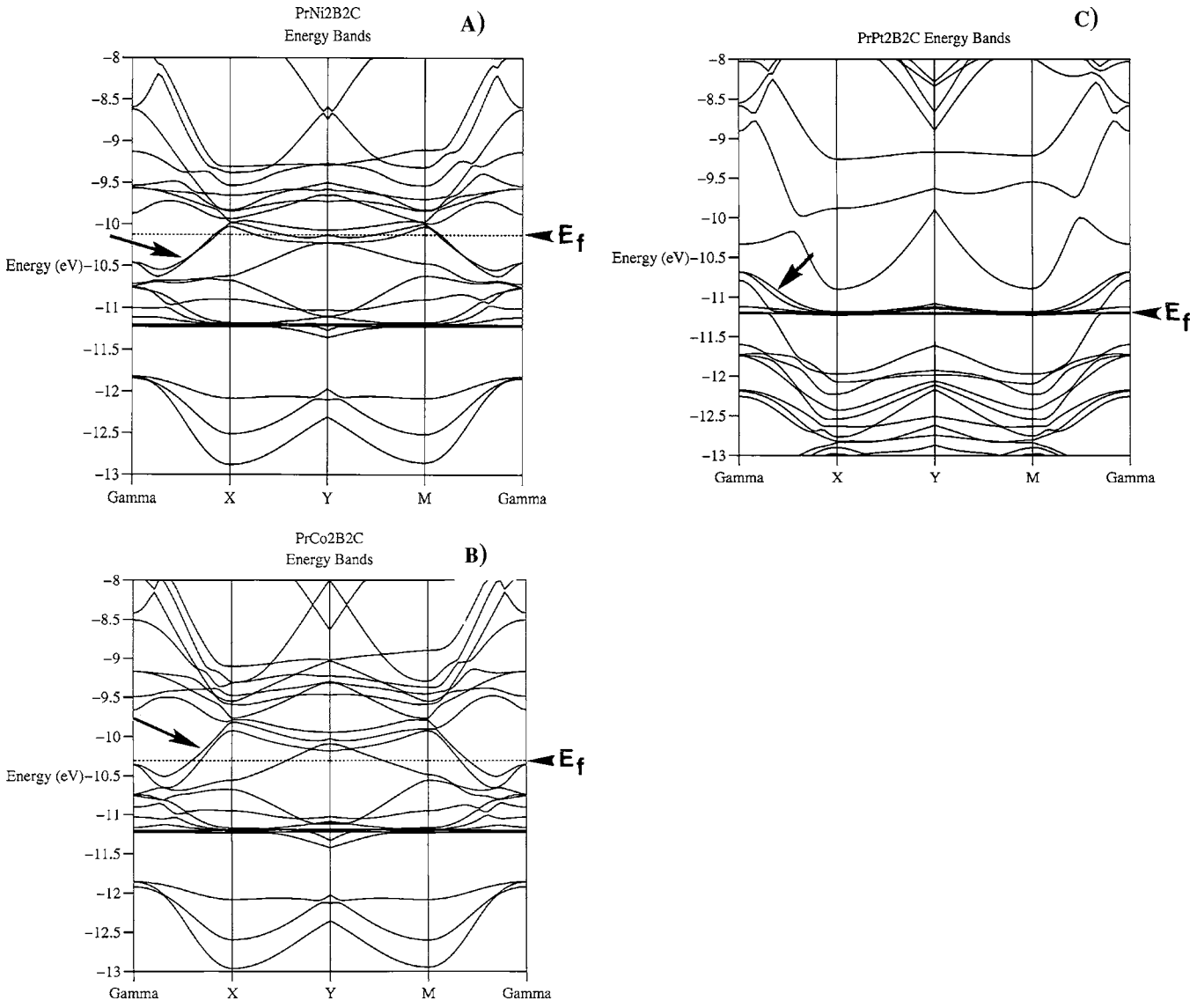

FIG. 2. (A)-(C) Band-structure calculations for $PrCo_2B_2C$, $PrNi_2B_2C$, and $PrPt_2B_2C$. The Fermi level is indicated by the dotted line.

compounds analyzed. The bands located at ≈ -11.2 eV belong to Pr $-f$ states, which are extremely flat, manifesting a saddle point extremum. This flatband produces a strong peak at E_f, as is the case for Lu superconductors.[6,7,23] The dispersion and the position at E_f of these flatbands depend strongly on the change of structural parameters. Finally, it was found that at about 11.8 eV a triply degenerated band belongs to the admixture of Pr, Co, C bands, in which slight differences are observed at the gamma point in Pr/Co.

On the other hand, the full isostructural substitution of Ni/Co by Pt significantly modified the dispersion diagrams of the same FBZ, as is depicted in Fig. 2(c). While for Pr/Ni and Pr/Co the Fermi energy was located at around -10.2 eV, for Pr/Pt is located at about -11.2 eV. Here the scenario is fully different, since a group of bands is highly localized along the Fermi energy. One group belongs to the Pt$-d$ states, and the contribution at the Fermi level is different to that of Pr/Ni(Co) bands. Here, the antibonding ddσ^* character is symmetrical in the Γ-X and M-Γ direction of the FBZ [arrow in Fig. 2(c)]. Also, it is possible to expect quasi-isotropic metallic scattering in this compound. The ddσ^* contribution of each band separately at the total DOS is as follows: Pt d_{x2-y2} contributes $\cong 2\%$ and $d_{z2} \leqslant 1\%$, with a total contribution of the order of $\cong 2$, in contrast to the Pr/Co ($\sim 13\%$) and Pr/Ni ($\sim 22\%$), even in the Ni-based superconductor compounds.[5,7] Another group belongs to the Pr $-f$ states, and it is seen as extended flatbands along the Fermi level. A totally different situation exists for the $-f$ bands for Pr/Ni(Co) compounds, which are localized in the valence band of their dispersion diagrams. This result suggests that not only the $-d$ electrons take part in the electronic transport, but also the $-f$ electrons. In other words, there is delocalization of the $-f$ electrons contributing to the metallic conduction in Pr/Pt compound.

B. Density of states

Total and projected density of states were calculated separately for Pr ($-f$, $-d$, $-p$, and $-s$), M=Ni, Co, Pt ($-d$, $-p$, and $-s$), B ($-p$ and $-s$), and C ($-p$ and $-s$), and are shown in

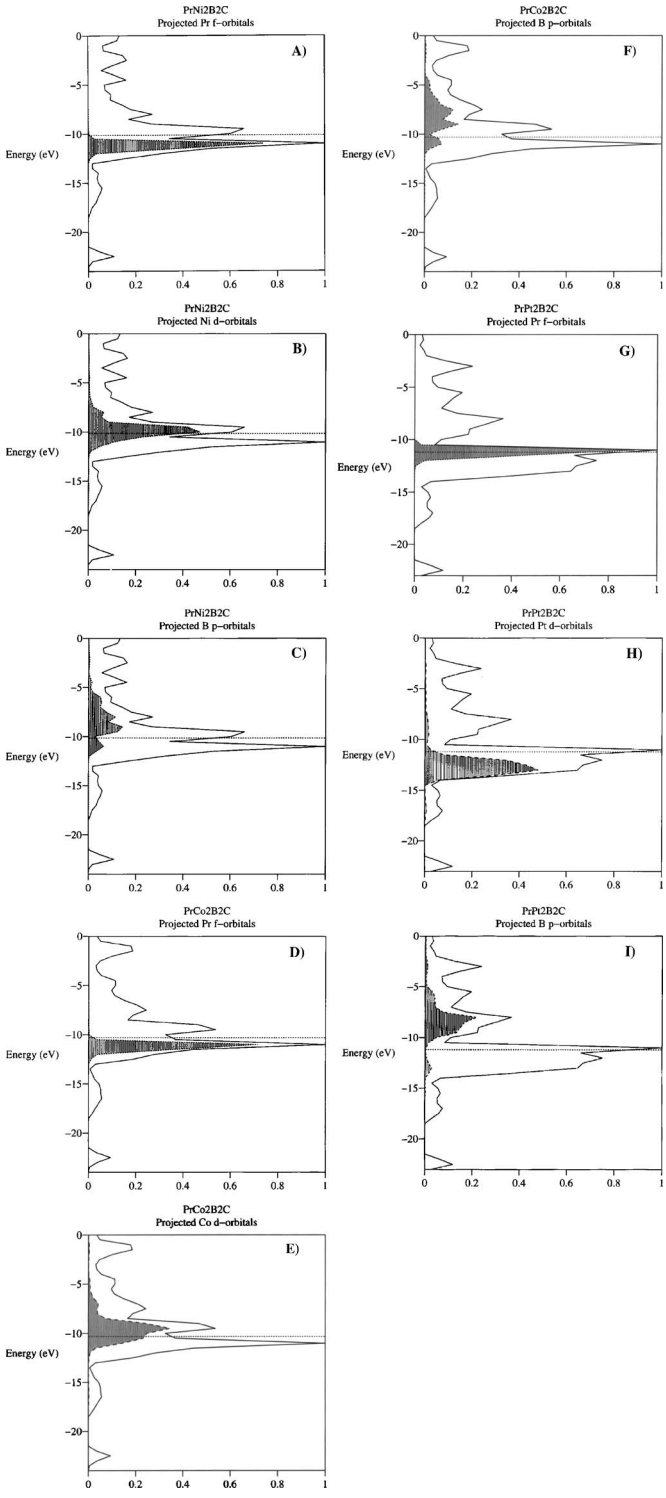

FIG. 3. (A)-(I) Total and projected DOS for $PrCo_2B_2C$, $PrNi_2B_2C$, and $PrPt_2B_2C$. The solid line indicates the total DOS, while the hatched lines correspond to the appropriate projected DOS for $-p$, $-d$, and $-f$ orbitals. The Fermi level is indicated by a horizontal dotted line.

Figs. 3(a)–3(c) for $PrNi_2B_2C$, Figs. 3(d)–3(f) for $PrCo_2B_2C$, and Figs. 3(g)–3(i) for $PrPt_2B_2C$, respectively. In these figures, the energy in electron volt units (vertical axis) is plotted vs percent contribution (horizontal axis); the solid line represents the total DOS while the dotted and hatched lines are the selected projected DOS for each orbital. In each graph the highest peak is selected as 100% contribution, while the other peaks are scaled with respect to the highest peak. The horizontal dotted line indicates E_f. Here, it is important to examine the different contributions to the total DOS in order to obtain an overview of the electronic transport properties in the vicinity of the Fermi level for each compound.

As expected, there are common characteristics in the shape and total orbitals contribution to the DOS, with a slight difference in the PDOS for $PrNi_2B_2C$ and $PrCo_2B_2C$, and as mentioned before, both are metallic but nonsuperconducting compounds. The projected orbitals crossing E_f are composed of Pr $-f$ states located below E_f and only a small tail diffuses above E_f, as observed in Pr/Co compound. The Ni and Co $-d$ states dominate the electron population at E_f, which contributes with ~33 and 20%, respectively. A small B $-p$ state contribution of ~2 and 5% and almost null C $-p$ states above E_f are observed. The total DOS is ~35 and ~26% for Pr/Ni and Pr/Co compound, respectively. The situation is completely different for $PrPt_2B_2C$. The projected orbitals crossing the Fermi level are composed primarily of Pr $-f$ states located above E_f and contributing with ~80%, Pt $-d$ states located below E_f, with a small contribution of the order of ~5%, and C $-p$ states contributing ≈9.5%, while the B $-p$ states contribution is null. The total contribution is ~85%.

We also observe that for nonsuperconducting compound, the Fermi energy falls in a pseudogap (valley) separated mainly by the Co, Ni $-d$ states and Pr$-f$ states, while for Pr/Pt a strong and sharp peak is seen in the total DOS near E_f. In this context, it has been proposed that the superconductivity occurs when special s-p bands are optimally aligned at the E_f, which is observed for nearly ideal NiB_4 angles in Y,Lu/Ni-based compounds, yielding high total DOS at $E_f \approx 75\%$.[9] In agreement with these characteristics, high total DOS at E_f is found for Pr/Pt. Here, the mayor contribution is due to the $-f$ states, with small contribution of Pt $-d$ states. This fact suggests that the population of this type of electrons is not a necessary condition to the superconducting to take place. However, from the crystallographic point of view, the nearly ideal NiB_4 angles seem to confirm that the tetrahedral angle is an important factor to the superconductivity, since this is ~106.6° (see Table II), quite similar to that found in $DyNi_2B_2C$ compound,[10] where superconductivity is about 6 K for Pr/Dy and Pr/Pt compounds. It is worthwhile emphasizing the role of −C state contribution to the total DOS. Mattheiss *et al.*[9] suggest conventional superconductivity for Ni-based compound, where the s-p states are strongly coupled to the high-frequency boron A_{1g} phonon mode. Here the superconductivity is likely associated to substantial contribution especially from the $C-p$ state, since its contribution is unexpectedly high at E_f.

More information regarding the hybridization for $PrNi_2B_2C$, $PrCo_2B_2C$, and $PrPt_2B_2C$ is provided in Figs. 4(a)–4(c). Figure 4(a) shows information of the total (solid line) and projected DOS (hatched lines) for $PrNi_2B_2C$. There, only those orbitals that contribute to the appropriate hybridization have been projected, as follows: Ni $-d$ contributes with ≈33%, Pr $-f$ with ≈3%, B $-p$ with ≈2%, and C

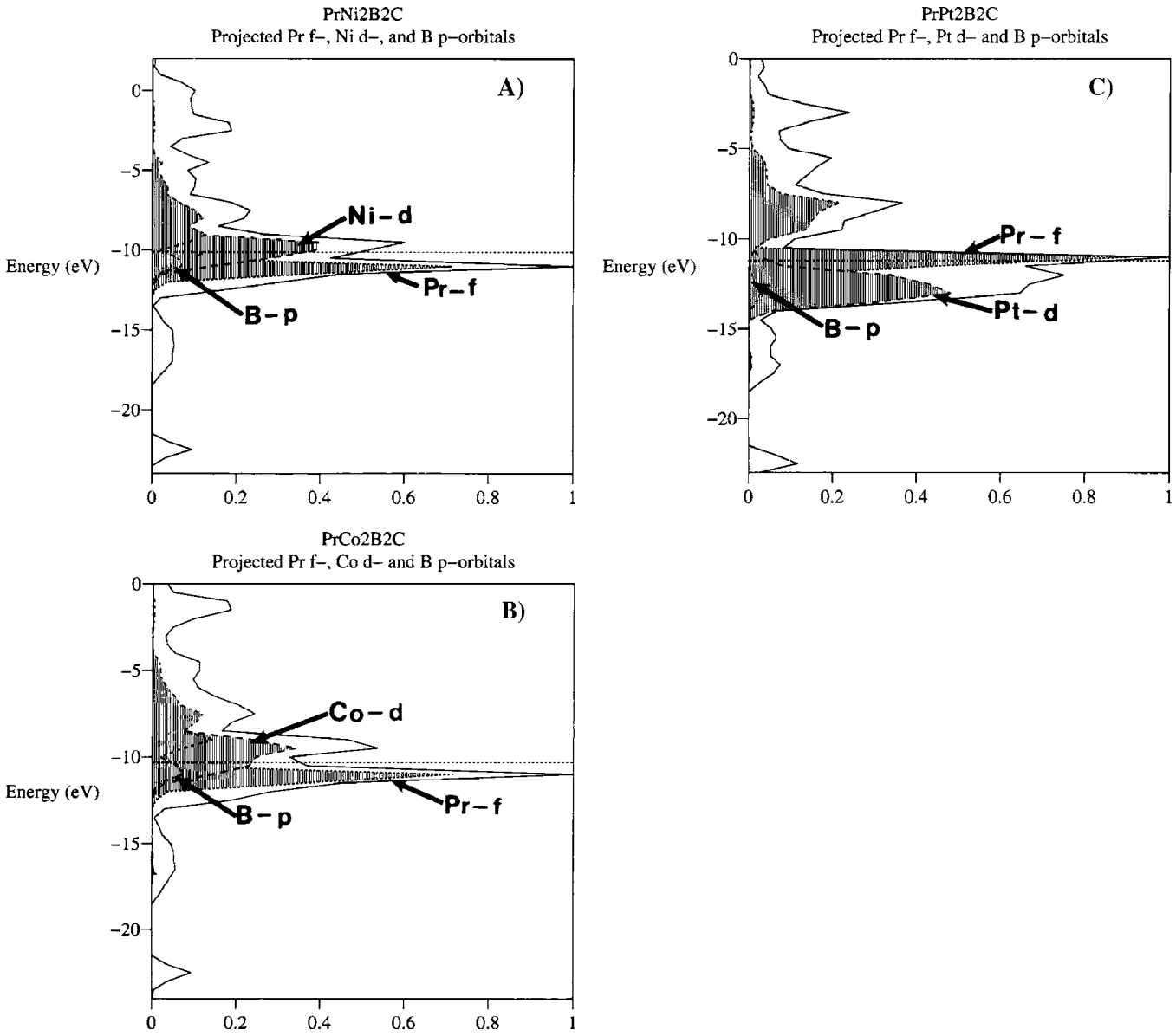

FIG. 4. (A)-(C) Total and projected DOS for the B $-p$, $M-d$, and Pr $-f$, overlapping in $PrCo_2B_2C$, $PrNi_2B_2C$, and $PrPt_2B_2C$ compound. The arrows indicate the appropriate DOS projected which contributes to the hybridization in each compound.

$-p$ with $\approx 2\%$. Notice that C contributions are not shown in the figure for the sake of clarity. For $PrCo_2B_2C$, the information regarding hybridization is provided in Fig. 4(b). There, the Co $-d$ contributes with $\approx 20\%$, Pr $-f$ with $\approx 5\%$, B $-p$ with $\approx 5\%$, and C $-p$ with $\approx 2\%$. Notice a similar hybridization for Pr/Ni and Pr/Co; consequently, similar transport behavior is expected in both compounds. Afterward, the information regarding hybridization for $PrPt_2B_2C$ is provided in Fig. 4(c). The Pt $-d$ contributes with $\approx 5\%$, Pr $-f$ with 73%, B $-p$ with almost null contribution, and C $-p$ with $\approx 9.5\%$. The fact that the $PrPt_2B_2C$ presents different hybridization (the atoms that form the unit cell contribute differently) corroborates the different electronic transport behavior that has been pointed out in the reported literature.[1,13,14,25]

An appreciable hybridization between the admixture of $-d$, $-p$ states crossing the E_F for Pr/Ni and Pr/Co compounds and the enhancement of the $-f$ band contribution with respect to the superconductor Lu/Ni, where in the latter compound the Lu $-f$ contribution only reaches 0.55%,[5] is manifested by the different experimental transport properties.[12,13] For example, the resistivity (ρ) as a function of temperature is linear down to ~ 100 K (metallic character). with major slope ($d\rho/dT$) values for Pr/Co compounds. Furthermore, the specific heat in this range of temperature is higher in Pr/Co with respect to Pr/Ni compounds.[13] The situation is very different in Pr/Pt compounds. Michor *et al.*[24] have reported that the normal state heat capacities in $LaPt_2B_2C$, $LaPt_{1.5}Au_{0.5}B_2C$, and $PrPt_2B_2C$ have a weak coupling of the electron-phonon factor (λ) which is not in line with the superconducting Y,Lu/Ni-based compounds.[25] These latter compounds have a low Sommerfeld constant γ (~ 15 mJ/mol K^2) and resistivity ($\sim 4-8$ $\mu\Omega$ cm) values just before Tc as a result of the predominant admixture of Ni $-d$ and B $-p$ states in the DOS at the E_f. In contrast, Pr/Pt has

TABLE III. Mulliken atomic orbital populations for Pr–f, $M-d$, B 2–p, and C2–p orbitals for $PrNi_2B_2C$, $PrCo_2B_2C$, and $PrPt_2B_2C$ crystals. M_1, M_2, B_1, and B_2 are the different atomic position environments in the M_2B_2 layer in the crystals.

		Pr–f orbitals					
	f_{z3}	f_{xyz}	$f_{y(3x2-y2)}$	$f_{z(x2-y2)}$	f_{yz2}	f_{xz2}	$f_{x(x2-3y2)}$
Pr/Ni	1.9994	1.9994	1.9964	1.9933	1.9906	1.9886	1.9870
Pr/Co	1.9981	1.9981	1.9961	1.9944	1.9987	1.9881	1.9885
Pr/Pt	0.2079	0.4391	0.4480	0.8625	0.1754	0.7978	0.8946
			$M-d$ orbitals				
		d_{yz}	d_{xy}	d_{xz}	d_{x2-y2}	d_{z2}	
	Ni_1	0.8981	0.8648	0.4480	0.6568	0.6512	
	Ni_2	0.3267	0.9638	0.6405	0.5938	0.6995	
	Co_1	0.7030	0.5877	0.3484	0.4898	0.4342	
	Co_2	0.5648	0.7229	0.5648	0.4042	0.3518	
	Pt_1	1.8133	1.9395	1.9345	1.9002	1.8561	
	Pt_2	1.9862	1.6320	1.8066	1.9190	1.8710	
			$B-p$ orbitals				
		p_x	p_y	p_z			
Pr/Ni	B_1	0.6978	0.5083	0.4872			
	B_2	0.0236	0.0134	0.1886			
Pr/Co	B_1	0.7263	0.5184	0.1387			
	B_2	0.0225	0.0157	0.1387			
Pr/Pt	B_1	0.2845	0.2678	0.075			
	B_2	0.0091	0.0134	0.0222			
			C $-p$ orbitals				
		p_x	p_y	p_z			
Pr/Co		1.5181	1.6636	1.4562			
Pr/Ni		1.5229	1.6372	1.4942			
Pr/Pt		1.4181	1.4646	1.3547			

higher values of both the $\gamma(\sim 35\ \mathrm{mJ/mol\ K^2})$ and resistivity ($24\ \mu\Omega\,\mathrm{cm}$) just before Tc. Two factors can influence the higher values of the ρ and γ in Pr/Pt with respect to those superconducting Y,Lu/Ni-based compounds.[25] On the one hand, the reduced mean-free path ($1\sim 18$ Å)[13,14] suggests a considerable enhancement of the interactions at E_f with respect to $Y/LuNi_2B_2C$ compound, at 1 to about 110 and 190 Å, respectively.[25] Another factor could have arisen from appreciable and predominant contribution of delocalized Pr $-f$ state plus Pt$-d$ and C$-p$ states weakly hybridized with respect to Y,Lu/Ni compound.

At low temperature ($T<100$ K), the transport behavior is dominated by incoherent crystalline electric field (CEF) scattering for Pr/Ni and PrCo [26] and non-Kramer singlet state for Pr/Pt compound.[14] It is worthwhile mentioning that in our calculations we did not include electronic correlation effects in a formal mathematical sense. Instead are included throughout the Huckel coefficients H_{ij} (ionization potential for each atom) obtained from experimental values (when available) or from most accurate *ab initio* calculations. Thus, neither CEF nor spin-orbit interactions were considered, except as mentioned before, throughout H_{ij}. For the three compounds under investigation, these terms are important with a subsequent splitting of some energy bands at some highly symmetric points in the FBZ. These effects will be considered in future investigations.

C. Mulliken analysis and crystal orbital overlapping population

Mulliken population analysis is defined as indices to quantitatively locate electronic charge around an atom and its bonding or antibonding nature.[27] In our analysis it is interesting to analyze the charge distribution around the Fermi level. The atomic charge distribution for Pr 4f, M 3d, B 2p, and C 2p orbitals is shown in Table III for each compound. The values provide the electronic occupation, two being the maximum number of electrons in a single orbital. It is clearly seen for the Pr/Ni and Pr/Co that the Pr $-f$ orbitals, f_{z3}, f_{xyz}, $f_{y(3x2-y2)}$, $f_{z(x2-y2)}$, f_{yz2}, f_{xz2}, and $f_{x(x2-3y2)}$, each one is more than half filled. The charge distribution of the $-f$ orbitals should be located below the E_f, as is clearly seen in the total and PDOS in Figs. 3(a) and 3(d). The contrary happens in Pr/Pt, where each $-f$ orbital is lightly located above E_f [Fig. 3(g)]. There, these $-f$ orbitals are less than one half filled, yielding minimum and maximum occupation of 0.20 and

TABLE IV. Average net charge from Mulliken population analysis for Pr/Ni, Pr/Co, and Pr/Pt crystal.

$PrNi_2B_2C$		$PrCo_2B_2C$		$PrPt_2B_2C$	
Pr	−10.9448	Pr	−10.9071	Pr	−0.4919
C	−2.28437	C	−2.2278	C	−1.8769
Ni_1	+6.0361	Co_1	+5.9934	Pt_1	+0.1809
Ni_2	+6.3428	Co_2	+6.2714	Pt_2	+0.1490
B_1	−0.1859	B_1	−0.1910	B_1	+0.8941
B_2	+1.0362	B_2	+1.0611	B_2	+1.1447

0.89 for fz^3 and $f(x^2-y^2)$ orbitals, respectively. The atomic charges for the M atoms also show remarkable changes in the charge distribution on the $-d$ orbitals. Here, two different types of M_1-B_1 and M_2-B_2 atoms are stacked along the c axis. While Ni and Co show identical filled $-d$ orbitals, the charge environment is fully different in the Pt atom. Hence, the antibonding states ($d_{(x2-y2)}$, d_{z2}) are slightly more filled for Ni than Co compound, but both e_g and t_{2g} (d_{zx}, d_{xy}, d_{xz}) orbitals are less than one half filled. The corresponding boron band filling also shows the $-p$ orbitals less than one half filled, being almost empty for B_2-p_x, p_y, and p_z orbitals. In Pr/Pt, both e_g and t_{2g} for Pt_1 and Pt_2 orbitals are almost filled with corresponding B $-p_x$, p_y and p_z almost empty. This means that the charge distribution of Pt $-d$ orbitals should be located in the valence band (below E_f) and the B $-p$ orbitals above E_f, as seen in Figs. 3(h) and 3(i). Finally, the charge population for C $-p$ orbitals is more than half filled for the three crystals, suggesting that the C $-p$ charge populations are homogenously distributed in the Pr-C layer, being the difference between the $-f$ orbitals.

It is important to note that Pt $-d$ orbitals have two electrons without the possibility that unfilled $-d$ orbitals lead to magnetic moments from this layer. Similar behavior has been found in YNi_2B_2C, where specific heat and susceptibility measurements[29] claimed that the Ni $-d$ orbitals are almost completely filled, corroborating the nonmagnetic character of the Ni atoms in the structure. Here, in some sense to explain the nonmagnetic nature of the Pt_2B_2 layer in contrast to what happens in Pr/Co and Pr/Pt, where there is an unfilled $-d$ band in $(Ni,Co)_2$-B_2, could be the source of the magnetic moment. Recent results in Pr/Ni and Pr/Co showed two magnetic anomalies (at 15 and 150 K), which could be due to the weak ferromagnetic order arising from this M_2B_2 layer.[13] This is an interesting point that deserves further investigation, since in this plane the absence of the superconductivity could be related to some magnetic signal in this layer.

The average atomic net charge for the three compounds determined from Mulliken population calculation is listed in Table IV. These values give a measure of the degree of bonding between nearby atoms. Positive bond order indicates a bond between atoms, and negative bond orders indicate that the atoms repel each other (antibonding interaction). Several important aspects can be pointed out from Table IV. Notice the similar values of the average net charge for each atom in both $PrCo_2B_2C$ and $PrNi_2B_2C$ compound, with small variations in the bond order for some specific atoms. We note that the average net charge in Pr and C atoms is negative, leading to antibonding interaction on this layer for the three compounds. This antibonding nature is consistent with the results found in YNi_2B_2C superconductor compounds.[30] In Ni(Co)-B layers, average atomic charge displays similar values, with similar impact in the electronic structure. For example, in Pr/Ni and Pr/Co the atomic orbital populations are not homogeneously distributed between the M-B atoms. Here, in both compounds some discrepancies are clearly observed, occurring in the sign of B_1 average net charge. These results indicate ionic charge transfer from B_1 to Ni_1 and Co_1 atoms, in contrast to what occurs in Pt-B atoms where the positive sign in M_2B_2 preserves the net charge between the Pr-C layer and M_2B_2 layers in the cell. As we can see, the average net charge analysis shows different charge distributions, corroborating the different nature of Ni(Co)-based compounds with those of Pt-based compounds. Nonetheless, for $PrPt_2B_2C$, the positive and negative charges are further homogeneously distributed along the crystals, since the negative net charge is localized in the Pr-C atoms, which maintain crystal neutrality through the positive net charge in the Pt_2B_2 layers.

A quantitative picture of average net charge and bonding nature considering the minimum distance between Pr-C, M-M, B-C, and the M-B layers can be obtained using Mulliken population as well as COOP. The integral of the COOP curves gives the total overlap population, which is not identical to the bond order but scales like it.[28] The amplitude of the curve depends on the number of states in that specific interval, the magnitude of the coupling overlap, and the size of the coefficients in the molecular orbital under consideration. Additional information is provided by the sign obtained from the calculation. Also, positive or negative charge provides bonding or antibonding states in the crystal atomic distribution.

Figures 5(a)–5(c) show the COOP curve around the M-M bonds for the three compounds. There, energy (in electron volts) is plotted vs positive (bonding) or negative (antibonding) contribution (in percent) from each orbital and each band. It is quite clear that the bonding-antibonding contribution for Ni_1-Ni_2 ($d_{Ni1\text{-}Ni2}$=2.616 Å) and Co_1-Co_2 ($d_{Co1\text{-}Co2}$=2.5566 Å) bonding are quite similar. This is not surprising because of the PDOS described in Sec. III B, and the structural differences described in Sec. II are quite small in both compounds. The antibonding states are spread above the Fermi level, with remarkable differences at energies from −2 to 14 eV; however, it is important to concentrate on those contributions on bonding-antibonding at the Fermi level. The

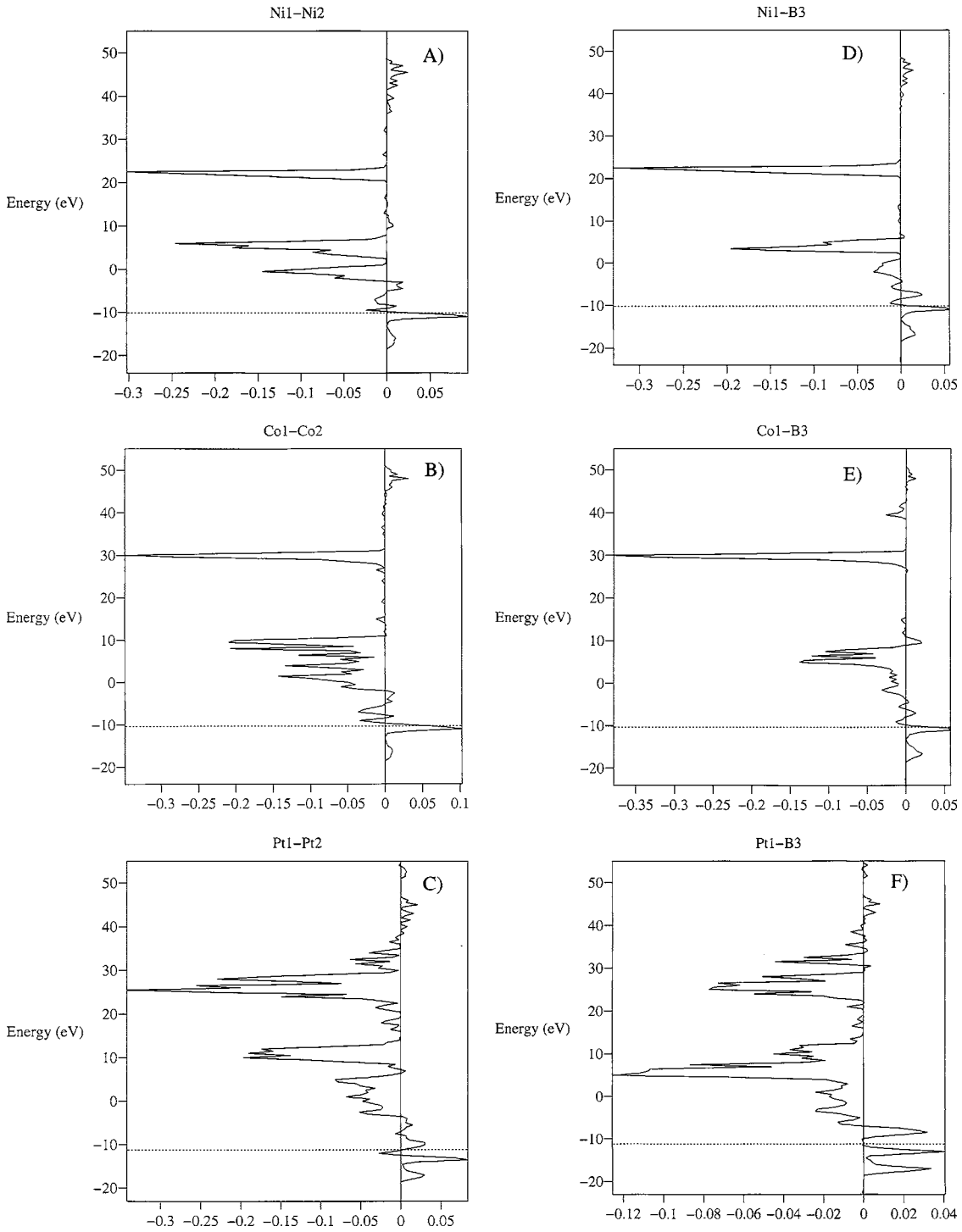

FIG. 5. (A)–(C) The crystal orbital overlap population around the $M1$-$M2$ atoms. (D)–(F) The COOP for M_1-B_3 layer in PrM_2B_2C with M=Ni, Co, and Pt.

$-d$ states fall in bonding character for Pr/Ni and Pr/Co compound, as seen in Figs. 5(a) and 5(b). The opposite situation is observed in Pt_1-Pt_2 bonding, where E_f falls close to the antibonding states, as seen in Fig. 5(c). Here, the nearly antibonding state means that the Pr/Pt tends to structural instability, since the Pt-Pt distance ($d_{Pt\text{-}Pt}$=2.7174 Å) becomes shorter than the Pt metallic fcc structure. We now turn our attention to the COOP curves around the $M-d$ and B $-p$ states, since the intensity of the hybridization takes place on the p-d overlapping for each compound. Figures 5(d) and 5(e) show the COOP curves for Ni_1-B_3, Co_1-B_3, and Pt_1-B_3. There, if the hybridization occurs, it will be manifested in the area of that bonding-antibonding contribution around the Fermi level. For the two first compounds, E_f falls in bonding with similar areas, while the Pr/Pt falls in a gap, that is, for this last compound, the hybridization is null compared to the Pr/Ni(Co) compound. Finally, we can observe clearly that the more extended Pt$-5d$ orbitals compared with the

Ni,Co−3*d* orbitals produce a remarkable geometrical change of atomic arrangements between atoms, inducing modifications in the charge distribution and COOP antibonding-bonding character.

IV. CONCLUDING REMARKS

From the calculations described herein, the following conclusions about $PrCo_2B_2C$, $PrNi_2B_2C$, and $PrPt_2B_2C$ can be drawn. The calculated energy bands indicate that the three compounds under investigation show quasi-isotropic metallic behavior. For Pr/Ni and Pr/Co, the electronic structure is quite similar indicating that the Ni(Co) *d* bands located at the Fermi energy are the principally responsible of the metallic behavior. From the total and PDOS, as well as the overlapping at E_f, it was possible to identify the contributions from each orbital of each atom and the degree of the $-p$, $-d$, and $-f$ hybridization. The hybridization is strong and similar for Pr/Ni and Pr/Co, while the covalence between the extended Pt 5*d* and B, C $-p$ states is weak. In Pr/Ni(Co) E_f falls in a valley, while for Pr/Pt E_f is located in a crest. Mulliken population analysis indicates identically filled $-f$ and $-d$ orbitals for Pr/Ni(Co), while the charge electronic population environment for $-f$ and $-d$ orbitals is fully different for Pr/Pt compounds. Here, the Pt−*d* orbitals are almost filled, without probability that the Pt_2B_2 layer lead to magnetic moment as a consequence of unfilled $-d$ orbitals; in contrast, for Pr/Ni(Co) compounds the unfilled −d orbitals strongly suggest a magnetic moment arising from these orbitals inside of the $Ni(Co)_2B_2$ layer. Furthermore, average net charge in Pr/Ni(Co) shows charge transference between Ni(Co)-B layers, which it is not in line with the Pr/Pt superconductor compound. Thus, these theoretical evidences suggest that the absence of superconductivity in Pr/Ni and Pr/Co are connected by the remarkable instabilities between $-d$, $-p$ and $-f$ states with respect to that observed in the superconductor $PrPt_2B_2C$ compounds.

ACKNOWLEDGMENTS

D.H.G. acknowledges A. Aparicio, M. Sainz, and J. Peralta for technical support. A. Duran thanks the Retencion Program supported by CoNaCyT, S. Bernés for the x-ray analysis and F. Silvar and J. Palomares for their technical help.

[1] K. H. Muller and V. N. Narozhnyi, Rep. Prog. Phys. **64**, 943 (2001).
[2] H. Eisaki, H. Takagi, R. J. Cava, B. Batlogg, J. J. Krajewski, W. F. Peck, Jr., K. Mizuhashi, J. O. Lee, and S. Uchida, Phys. Rev. B **50**, 647 (1994).
[3] R. J. Cava, H. Takagi, H. W. Zandbergen, J. J. Krajewski, W. F. Peck, Jr., T. Siegrist, R. B. Van Dover, R. J. Felder, K. Mizuhashi, J. O. Lee, H. Eisaki, and S. Uchida, Nature (London) **367**, 146 (1994).
[4] E. Tominez, E. Alleno, P. Berger, M. Bhon, C. Mazumdar, and C. Godart, J. Solid State Chem. **154**, 114 (2000).
[5] L. F. Mattheiss, Phys. Rev. B **49**, 13279 (1994).
[6] W. E. Pickett and D. J. Singh, Phys. Rev. Lett. **72**, 3702 (1994).
[7] M Divis, K. Schwarz, P. Blaha, G. Hilscher, H. Michor, and S. Khmelevskyi, Phys. Rev. B **62**, 6774 (2000).
[8] C. Felser, J. Solid State Chem. **160**, 93 (2001).
[9] L. F. Mattheiss, T. Siegrist, and R. J. Cava, Solid State Commun. **91**, 587 (1994).
[10] J. W. Lynn, S. Skanthakumar, Q. Huang, S. K. Sinha, Z. Hossain, L. C. Gupta, R. Nagarajan, and C. Godart, Phys. Rev. B **55**, 6584 (1997).
[11] R. J. Cava, B. Batlogg, T. Siegrist, J. J. Krajewski, W. F. Peck, Jr., S. Carter, R. J. Felder, H. Takagi, and R. B. van Dover, Phys. Rev. B **49**, 12384 (1994).
[12] M. El Massalami, H. A. Borges, H. Takeya, R. E. Rapp, and F. A. B. Chaves, J. Magn. Magn. Mater. **279**, 5 (2004).
[13] A. Durán, S. Bernès, and R. Escudero, Phys. Rev. B **66**, 212510 (2002); A. Duran, S. Bernes, R. Falconi, O. Laborde, and R. Escudero Phys. Rev. B **74**, 134513 (2006).
[14] S. K. Dhar, A. D. Chinchure, R. Nagarajan, S. M. Pattalwar, L. C. Gupta, E. Alleno, and C. Godart, Phys. Rev. B **65**, 132519 (2002).
[15] A. Durán, E. Muñoz, S. Bernès, and R. Escudero, J. Phys. Condens. Matter **12**, 7595 (2000).
[16] M. H. Whangbo and R. Hoffmann, J. Am. Chem. Soc. **100**, 6093 (1978).
[17] R. Hoffmann, J. Chem. Phys. **39**, 1397 (1963).
[18] G. A. Landrum; the YAEHMOP package is freely available at http://overlap.chem.Cornell.edu:8080/yaehmop.html. $-f$ orbitals are included in the calculation as a version 3.x, using W. V. Glassey's routine.
[19] D. H. Galvan, J. Mater. Sci. Lett. **17**, 805 (1998).
[20] S. Alvarez, *Table of Parameters for Extended Huckel Calculations* (Universitat de Barcelona, March 1993).
[21] I. R. Fisher, J. R. Cooper, and P. C. Canfield, Phys. Rev. B **56**, 10820 (1997).
[22] R. E. Peierls, *Quantum Theory of Solids* (Oxford University Press, Oxford, 1972).
[23] R. Coehoorn, Physica C **228**, 331 (1994).
[24] H. Michor, T. Holubar, C. Dusek, and G. Hilscher, Phys. Rev. B **52**, 16165 (1995).
[25] K. D. D. Rathnayaka, A. K. Bhatnagar, A. Parasiris, D. G. Naugle, P. C. Canfield, and B. K. Cho, Phys. Rev. B **55**, 8506 (1997); M. El Massalami, H. A. Borges, H. Takeya, R. E. Rapp, and F. A. B. Chaves, J. Magn. Magn. Mater. **279**, 5 (2004).
[26] Allenspach and U. Gasser, J. Alloys Compd. **311**, 1 (2000).
[27] J. P. Lowe, *Quantum Chemistry* (Academic Press, San Diego, 1993).
[28] R. Hoffmann, *Solid and Surfaces: A Chemist's View of Bonding in Extended Structure* (VCH, Wenheim, 1998), p. 32.
[29] B. J. Suh, F. Borsa, D. R. Torgeson, B. K. Cho, P. C. Canfield, D. C. Johnston, J. Y. Rhee, and B. N. Harmon, Phys. Rev. B **53**, R6022 (1996); N. M. Hong, H. Michor, M. Vybotnov, T. Holubar, W. Perthold, G. Hilscher, and P. Rogl, Physica C **227**, 85 (1994).
[30] P. Ravindran, B. Johansson, and O. Eriksson, Phys. Rev. B **58**, 3381 (1998).
[31] W. Wolfsberg and L. Helmholtz, J. Chem. Phys. **20**, 837 (1952).